Control of a Magnetic Levitation System Using Modified Super Twisting Sliding Mode Control under Inductance and Resistance Uncertainties

Alfian Ma'arif
Department of Electrical and Information Engineering, Universitas Gadjah Mada, Yogyakarta, Indonesia | Department of Electrical Engineering, Universitas Ahmad Dahlan, Yogyakarta, Indonesia
alfianmaarif@ee.uad.ac.id

Oyas Wahyunggoro
Department of Electrical and Information Engineering, Universitas Gadjah Mada, Yogyakarta, Indonesia
oyas@ugm.ac.id (corresponding author)

Adha Imam Cahyadi
Department of Electrical and Information Engineering, Universitas Gadjah Mada, Yogyakarta, Indonesia
adha.cahyadi@ugm.ac.id

Received: 7 December 2025 | Revised: 1 February 2026 and 9 April 2026 | Accepted: 9 April 2026

 DOI: https://doi.org/10.48084/etasr.16773

ABSTRACT

This paper examines the position regulation of a nonlinear Magnetic Levitation System (MLS) in the presence of coil resistance and inductance uncertainties due to temperature-dependent variations. First, a nonlinear MLS model is formulated and rewritten via a nonlinear coordinate transformation into an equivalent canonical form to facilitate controller synthesis. Then, a Modified Super-Twisting Sliding Mode Control (MSTSMC) scheme is developed by combining an equivalent control component with a continuous higher-order sliding switching law to achieve robust tracking with reduced chattering. All results reported in this study are obtained from MATLAB/Simulink simulations. Under nominal conditions, the proposed MSTSMC achieves fast transient performance (a rise time of 0.0665 s, a settling time of 0.115 s, and an overshoot of 0.1761%) with negligible steady-state error. Robustness is further assessed by varying the resistance and inductance within specified uncertainty ranges. In these conditions, the MSTSMC maintains stable tracking with bounded error. Compared with Conventional Sliding Mode Control (CSMC), MSTSMC provides improved quantitative tracking performance, as reflected by lower error indices-Integral of Absolute Error (IAE), Integral of Squared Error (ISE), Integral of Time-weighted Absolute Error (ITAE), and Root Mean Square Error (RMSE)- and yields smoother control actions with reduced chattering. This is confirmed through control-effort and chattering-related measures (RMS control and energy-like measures). These results suggest that the MSTSMC is a practical and effective approach for MLS regulation under electrical parameter uncertainty.

Keywords-Magnetic Levitation System (MLS); sliding mode control; nonlinear control; super twisting; uncertainty

I. INTRODUCTION

A Magnetic Levitation System (MLS) uses electromagnetic force to levitate an object [1]. Considered a modern technology, it has two distinctive characteristics: no friction and no contact between the object and the system [2, 3], offering high efficiency [4]. Due to these advantages, the MLS system has many applications, including suspension [5], bearings [6], wind turbines [7], maglev trains [8], disease diagnostics [9], biological diagnostics [10], and biomedical applications [11], among others. Figure 1 shows an MLS system, which is an iron ball that levitates by an electromagnetic inductor [12]. The sensor measures the object's position (air gap between the object and the electromagnetic system), and the controller is a microcontroller or a computer. The driver is designed to amplify the control signal from the controller. The system must keep the object levitating by balancing the electromagnetic and gravitational forces acting on it. The electromagnetic force must be applied correctly so that the object can levitate stably at the desired position. Due to these characteristics, the system exhibits fast dynamics and highly unstable behavior [13]. The MLS is nonlinear due to the inductor's characteristics when the temperature increases,

causing the resistance and inductance to vary with temperature change [14]. Many controllers are used in MLS to keep objects in the air. These controllers can be either linear or nonlinear. However, due to the nonlinear characteristics, linear controllers such as PID/fractional order PID [15], state feedback control [16], and fuzzy control [17], are not suitable for systems without applied linearization in only the area of an operating point. Therefore, nonlinear controllers, including feedback linearization [18], backstepping [19], high-gain observers [20], passivity [21], synergetic control [22], and Sliding Mode Control (SMC) [23], are more suitable for this type of system.

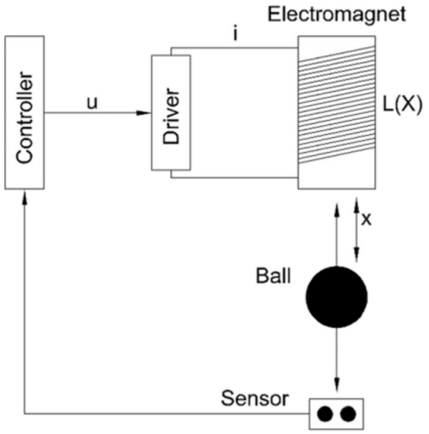

Fig. 1. The simplest MLS design.

The present research used SMC, which has advantageous characteristics such as high robustness and suitability for nonlinear systems [24]. SMC can be found in many systems, including induction motors [25], BLDC motors [26], quadrotors [27], quadcopters [28], inverted pendulums [29], mobile robots [30], Permanent Magnet Synchronous Motors (PMSMs) [31], coupled tank systems [32], grid systems [33], PMSGs [34], buck converters [35], and PMLS motors [36]. SMC delivers promising performance in linear and nonlinear systems. There are many types of SMC and modifications that improve the performance characteristics of augmented systems [37]. Previously proposed and designed types of SMC include Conventional Sliding Mode Control (CSMC) [38], integral SMC [39], global SMC [40], terminal SMC [41], fractional order SMC [42], higher order SMC [43], super twisting SMC [44], and integral super twisting SMC [45]. One problem with SMC is eliminating chattering in the control signal [46]. This research used and evaluated the system performance of the Modified Super-Twisting Sliding Mode Control (MSTSMC) implemented in the MLS model without chattering, contributing to the application of designing an MSTSMC. This design builds upon the standard super-twisting structure by augmenting the switching law with an additional sign. The present research also evaluates tracking and control-signal behavior under explicit resistance and inductance uncertainty caused by temperature variation. Additionally, it contributes to formulating the MLS model by employing a nonlinear coordinate transformation into an equivalent canonical form to facilitate transparent controller derivation and stability discussion. Finally, the effectiveness of the proposed MSTSMC is demonstrated through a comparative simulation study against CSMC under nominal and R–L uncertainty cases. Quantitative indices, such as time-domain specifications, tracking error metrics (IAE/ISE/ITAE/RMSE), and control-effort/chattering-related measures, are used to objectively substantiate performance improvements.

II. METHOD

A. Magnetic Levitation System Model

The system's dynamics can be analyzed using a mechanical and electrical approach, as shown in Figure 2. In this figure, R denotes resistance, L is inductance, F_g is gravitational force, F_e is electromagnetic force, x is the object's position relative to the inductor, e is source voltage, m is object mass, and i is current.

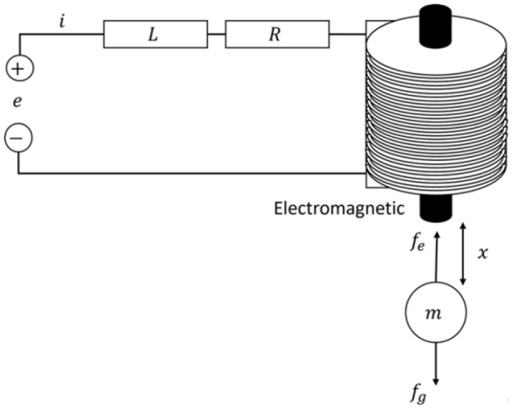

Fig. 2. The dynamics of MLS.

The dynamics of MLS can be written based on the mechanical analysis using the second Newton law:

$$m\ddot{x} = mg - f_e \tag{1}$$

where the electromagnetic force is expressed as:

$$f_e = -\frac{1}{2} i^2 \frac{d}{dx}(L(x)) \tag{2}$$

The inductance $L(x)$ is a nonlinear component that can be represented as:

$$L(x) = L + \frac{L_0 x_0}{x} \tag{3}$$

where L_0 is the constant inductance in the absence of the object, x_0 is the equilibrium reference position, and $L_0 x_0 = 2k$, with k being the electromagnetic constant, the electromagnetic force can be rewritten as:

$$f_e = k \frac{i^2}{x^2} \tag{4}$$

where:

$$k = \frac{L_0 x_0}{2} \tag{5}$$

The mathematical expression of MLS dynamics based on the mechanical analysis is:

$$\frac{d^2x}{dt^2} = g - \frac{k}{m}\left(\frac{i}{x}\right)^2 \tag{6}$$

The system can be analyzed using Kirchhoff's voltage law applied to its electrical components:

$$e = iR + \frac{d}{dt}L(x)i \quad (7)$$

Using simple mathematical procedures, (7) can be rewritten as:

$$\frac{di}{dt} = -\frac{R}{L}i - \frac{2k}{L}\frac{i}{x^2}\frac{dx}{dt} + \frac{1}{L}e \quad (8)$$

Therefore, the dynamics of MLS can be expressed as a state-space model by assuming $x_1 = x$, $x_2 = x'$, $x_3 = i$, and $u = e$. The MLS state-space dynamics are written as:

$$\dot{x}_1 = x_2; \quad \dot{x}_2 = g - \frac{kx_3^2}{mx_1^2} \quad (9)$$

$$\dot{x}_3 = -\frac{Rx_3}{L} + \frac{2kx_2x_3}{Lx_1^2} + \frac{u}{L} \quad (10)$$

with the output of the system:

$$y = x_1 \quad (11)$$

As can be seen in the MLS dynamics, the nonlinear characteristics can be observed in (10) and (11). A simpler model with only one dynamic equation showing nonlinearity can be achieved by transforming the model into an equivalent canonical form:

$$z_1 = x_1; \quad z_2 = x_2; \quad z_3 = g - \frac{kx_3^2}{mx_1^2} \quad (12)$$

where $x_1 > 0$ and $x_3 > 0$. Thus, an equivalent model in new coordinates can be expressed as:

$$\dot{z}_1 = z_2; \quad \dot{z}_2 = z_3; \quad \dot{z}_3 = f(z) + g(z)u \quad (13)$$

where:

$$f(z) = -\frac{4k^2x_2x_3^2}{mLx_1^4} + \frac{2kRx_3^2}{mLx_1^2} + \frac{2kx_3^2x_2}{mx_1^3} \quad (14)$$

$$g(z) = \frac{2kx_3}{mx_1^2L}u \quad (15)$$

and $x_1 > 0$. The nonlinear coordinate transformation in (12) rewrites the original MLS model in an equivalent canonical form (13). In nonlinear control/SMC design, this step provides a state evolution that follows a chain-like structure, with the control input explicitly appearing in an affine manner in the derivative of the sliding variable. Consequently, deriving the sliding function, equivalent control, and robust switching component becomes straightforward and analytically tractable while grouping the system nonlinearities into fewer terms. Temperature changes affect coil winding resistance and magnetic circuit properties, resulting in uncertainty of R and L. This work models resistance variation using the standard copper-temperature relation:

$$R(T) = R_o[1 + a(T - T_0)] \quad (16)$$

where $\alpha \approx 0.00393/°C$ at $20°C$. Therefore, a temperature rise ΔT corresponds to $\Delta R/R_0 \approx \alpha\Delta T$. For example, $\Delta T = 50°\text{C}$ yields $\approx 19.7\%$ increase in R, whereas $\Delta T = 60°\text{C}$ yields $\approx 23.6\%$. Since inductance (L) is proportional to the effective permeability of the magnetic circuit (μ_e), it changes with temperature. Additionally, practical magnetic circuits may experience shifts in inductance due to temperature-dependent core properties and operating effects, such as saturation. Therefore, an inductance (L) uncertainty range consistent with temperature and permeability variation is defined, as well as additional modeling mismatch, evaluating controller efficiency over these ranges.

B. Conventional Sliding Mode Control

The control system block diagram is shown in Figure 3. The SP block represents the set point, or reference value, while the error is the difference between the set point and the feedback from the sensor. The MLS block consists of the obtained MLS model and represents the MLS plant. The SMC is the designed sliding mode control, and the output is the object position.

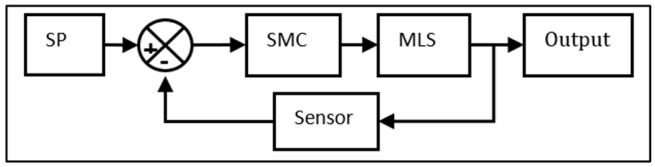

Fig. 3. Control system block diagram.

The first step in designing SMC is to design the sliding surface. The error sliding surface can be determined as:

$$e = z_1 - z_{1d} \quad (17)$$

$$\dot{e} = z_2 - z_{2d} \quad (18)$$

$$\ddot{e} = z_3 - z_{3d} \quad (19)$$

where z_{1d}, z_{2d}, z_{3d} are the reference values or the desired air gap, momentum, and flux. The model of the system has three state variables, so the sliding surface is determined as:

$$s = c_1e(t) + c_2\dot{e}(t) + \ddot{e}(t) \quad (20)$$

where c_1 and c_2 must satisfy the Hurwitz condition $c_{1,2} > 0$. The sliding surface parameters, c_1 and c_2, are chosen so that the polynomial associated with the reduced-order error dynamics on the sliding manifold is Hurwitz, providing stable internal motion once $s = 0$. In practice, c_1 and c_2 are chosen as positive constants to shape the desired convergence rate. Larger values result in a faster response, but require more control effort. The derivative of the sliding surface, s, can be defined as:

$$\dot{s} = c_1\dot{e}(t) + c_2\ddot{e}(t) + \dddot{e}(t) \quad (21)$$

Then, the Lyapunov function can be mathematically written as:

$$V = \frac{1}{s}s^2 \quad (22)$$

and its derivative is expressed as:

$$\dot{V} = s\dot{s} \quad (23)$$

By considering (21), it can be rewritten as:

$$\dot{s} = c_1\dot{e}(t) + c_2\ddot{e}(t) + f(z) + g(z)u - \dot{z}_{3d}(t) \quad (24)$$

Then, by substituting $\dot{x}_3$ in (22) into (23), an equation of the first derivative of the Lyapunov function can be obtained, as:

$$\dot{V} = s[c_1\dot{e}(t) + c_2\ddot{e}(t) + f(z) + g(z)u - \dot{z}_{3d}(t)] \quad (25)$$

The SMC signal consists of equivalent control and switching control. The control signal can be mathematically written as:

$$u = \frac{1}{g(z)}(-f(z) - c_1\dot{e}(t) - c_2\ddot{e}(t) + \dot{z}_{3d}(t) + u_{sw}) \quad (26)$$

where u_{sw} is the switching control:

$$u_{sw} = -\eta\, sgn(s) \quad (27)$$

where η is the constant and:

$$sgn(s) = \begin{cases} 1, & s > 0 \\ 0, & s = 0 \\ -1, & s < 0 \end{cases} \quad (28)$$

By substituting the control signal and switching control into the derivation of the Lyapunov function, it can be rewritten as:

$$\dot{V} = s\big(-\eta\, sgn(s)\big) = -\eta|s| < 0 \quad (29)$$

This shows that $\dot{V}$ is negative definite for s ≠ 0, while the parameter η is positive, meaning that the system is asymptotically stable in the sense of the Lyapunov function.

C. Modified Super Twisting Sliding Mode Control Design

Classical Super-Twisting Sliding Mode Control (STSMC) is typically formulated as a two-component structure: a super-twisting term proportional to $|s|^{1/2}\, sgn(s)$ plus an auxiliary term generated by an integral-like internal dynamic. In this work, a modified switching law is proposed that introduces an additional $sgn(s)$-dependent component and an extra tuning gain, giving a three-component switching law. This additional term provides an extra degree of freedom to shape the reaching dynamics and improve robustness when the coil's electrical parameters (resistance *R* and inductance *L*) vary with temperature. Thus, the proposed controller is not merely an implementation of standard STSMC; rather, it is a modified structure with an added control component and gain specifically motivated by and evaluated under *R–L* uncertainty in the MLS model. The switching control (u_{sw}) for the MSTSMC can be written as:

$$u_{sw} = -k_1|s|^{0.5}sgn(s) - k_2 sgn(s) + u_1 \quad (30)$$

$$\dot{u}_1 = -k_3 sgn(s) \quad (31)$$

or:

$$u_{sw} = -k_1|s|^{0.5}sgn(s) - k_2 sgn(s) - k_3\int sgn(s)d(t) \quad (32)$$

where $k_2 sgn(s)$ is the modification made in super twisting sliding mode control compared with super twisting sliding mode control (without $k_2 sgn(s)$). The CSMC gain is selected to control bounded matched uncertainties/disturbances, and the MSTSMC gains are chosen according to super-twisting robustness conditions to ensure finite-time convergence without chattering. Since *R–L* variations are the dominant uncertainty in this study (as tested in the uncertainty simulations), the gains are tuned to maintain stability and tracking performance across the specified parameter ranges. Substituting the control signal and switching control into the Lyapunov function derivation yields:

$$\dot{V} = s\left(-k_1|s|^{0.5}sgn(s) - k_2 sgn(s) - k_3\int |s|d(t)\right) = -k_1|s|^{0.5}|s| - k_2|s| - k_3|s|\int d(t) \quad (33)$$

This shows that $\dot{V}$ is negative definite, and the parameters k_1, k_2, and k_3 are positive, meaning that the system is asymptotically stable in the sense of the Lyapunov function.

III. RESULTS AND DISCUSSION

The following MLS parameters were used in the present study: the coil inductance was L = 0.12 H and the resistance was R = 9 Ω. The object mass was m = 0.36 g and the coil constant was k = 0.00013, whereas the gravitational force constant was g = 9.8 m/s². The research simulation was performed using MATLAB 2018. The performance analysis included time-domain response specifications, such as rise time (t_r), settling time (t_s), overshoot (O_s), and Steady-State Error (SSE). The tracking-error parameters (IAE, ISE, ITAE, and RMSE) are:

$$IAE = \int_0^T |e(t)|dt\,; \quad ISE = \int_0^T e^2(t)dt;\ ITAE = \int_0^T t|e(t)|dt\,;\ RMSE = \sqrt{\frac{1}{T}\int_0^T |e^2(t)|dt} \quad (34)$$

The control effort is quantified using RMS control (u_{RMS}) and energy-like measures (E_u) as:

$$u_{RMS} = \sqrt{\frac{1}{T}\int_0^T |u^2(t)|dt} \quad E_u = \int_0^T u^2(t)dt \quad (35)$$

A chattering-related measure based on total variation was used:

$$TV(u) = \int_0^T \dot{u}^2(t)dt \quad (36)$$

A. System Response in Initial Condition

In Figure 4, the black line is the reference value, the blue line is the response from the MSTSMC, and the red line is the response from the CSMC. The controller parameters were selected to ensure stability while balancing convergence speed and control effort. The sliding-surface coefficients c_1 and c_2 were chosen such that the characteristic polynomial associated with the reduced-order error dynamics on the sliding manifold was Hurwitz. For the second-order case, selecting $c_1 > 0$ and $c_2 > 0$ ensured stability; however, larger values increased the convergence rate at the expense of higher control activity. For the CSMC, the switching gain, η, was sufficiently large to satisfy the reaching condition in the presence of bounded matched uncertainties. Increasing η improves robustness, but it may also increase chattering and control effort. The final gains used for the CSMC parameter simulation were c_1 = 1000, c_2 = 80, and η = 300, which provide clear reaching behavior. For MSTSMC, the gains (k_1, k_2, k_3) were tuned to achieve chattering-free convergence. Generally, k_1 primarily influences convergence speed near the sliding surface through the $|s|^{1/2}\, sgn(s)$-type action. k_2 strengthens robustness against matched uncertainty, and k_3 shapes the internal super-twisting dynamics and the smoothness of the control signal. The final gains used in the simulations were chosen to maintain stable tracking

under nominal and *R–L* uncertainty cases while keeping the control signal smooth. The MSTSMC parameters were k_1 = 300, k_2 = 1, k_3 = 0.1, c_1 = 2000, and c_2 = 80. According to Table I, the CSMC and MSTSMC systems achieved the reference; MSTSMC showed a slightly better response than CSMC. The MSTSMC's detailed system performance specifications were 0.0665 s rising time, 0.1150 s settling time, and 0.1761% overshoot. Meanwhile, the CSMC-augmented system had a rising time of 0.1506, a settling time of 0.2874, and an overshoot of 0.00089%.

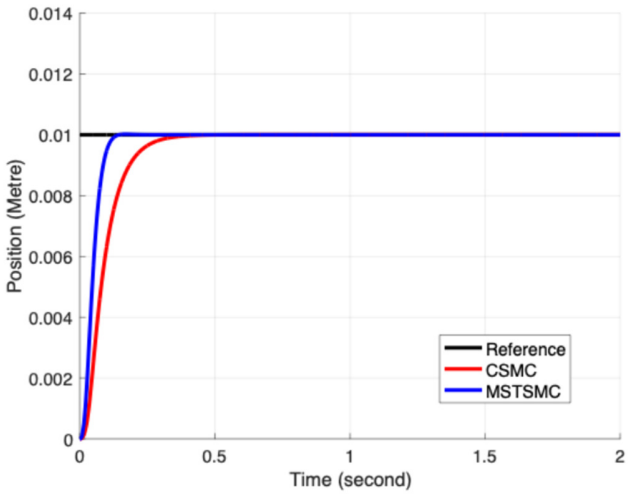

Fig. 4. Simulation results of CSMC and MSTSMC.

TABLE I. RESPONSE SYSTEM COMPARISON

Controller	t_r (s)	t_s (s)	O_s (%)	ss_e (m)
CSMC	0.1506	0.2874	0.00089	0
MSTSMC	0.0665	0.1150	0.1761	0

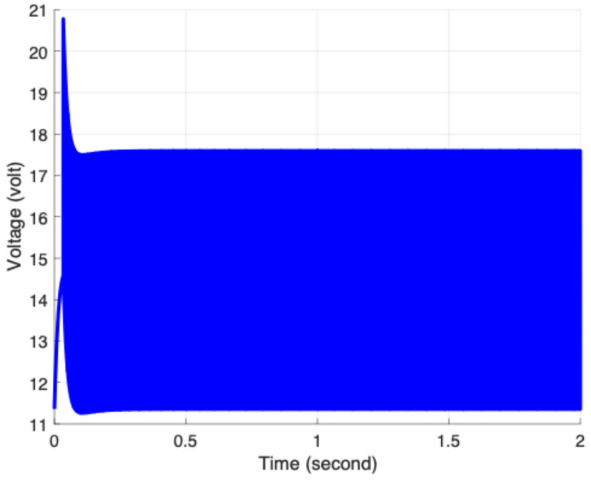

Fig. 5. Control signal of CSMC.

The control signal is depicted in Figures 5 and 6. Chattering was only observed in the control signal of the system with CSMC. The MSTSMC did not result in chattering. As observed, the MSTSMC had a more stable control signal. Based on Table II, the MSTSMC had smaller error values regarding IAE, ISE, ITAE, and RMSE than the CSMC.

In terms of control effort, the MSTSMC required a smaller value than the CSMC. The MSTSMC indicated smaller chattering because the total variations were smaller than those of the CSMC.

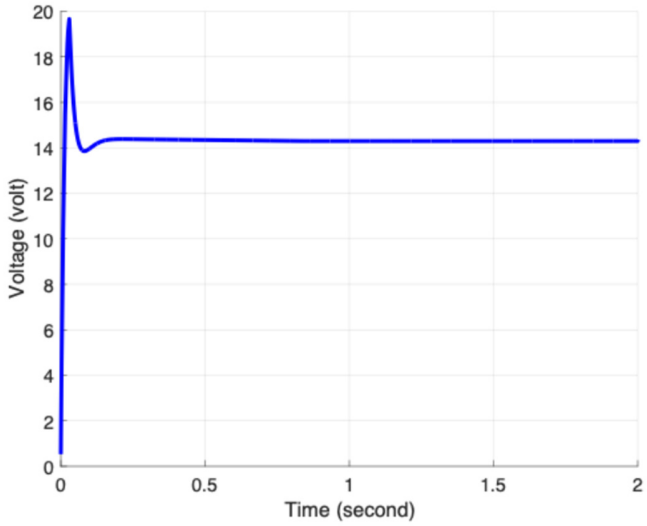

Fig. 6. Control signal of MSTSMC.

TABLE II. PERFORMANCE METRICS COMPARISON

Controller	*IAE*	*ISE*	*ITAE*	*RMSE*	u_{RMS}	E_u	*TV*
CSMC	6.235e-06	9.662e-04	6.903e-05	0.0303	14.8030	436.4	46.29
MSTSMC	3.558e-06	5.02e-04	1.698e-05	0.0222	14.3747	420.1	18.19

B. System Response with Uncertainty

To demonstrate robustness, this study expanded the uncertainty analysis from a single case to a parameter sweep study across the defined R and L ranges. The controllers on a grid of R and L combinations were measured, and the worst-case and average tracking indices (IAE, ISE, ITAE, and RMSE) as well as the control effort metrics (u_{RMS} and $\int u^2 dt$) were reported for all cases. This approach provides a reproducible robustness assessment. In the simulation, the MLS parameters were changed from their default values. The resistance value changed from R = 9 Ω to R = 7.5 Ω. The inductance value changed from L = 0.12 H to L = 0.24 H. In real-time practical use, an increase or decrease in system temperature causes a change in the parameter value or its uncertainty. According to Figure 7 and Table III, both systems achieved the reference when applied with CSMC and MSTSMC; however, the MSTSMC results were slightly superior to the CSMC results. The detailed system performance specifications for MSTSMC were 0.0665 s rising time, 0.1150 s settling time, and 0.1762% overshoot. Meanwhile, the CSMC results were 0.1506 s rising time, 0.2875 s settling time, and 0% overshoot. The control signals are displayed in Figures 8 and 9. The CSMC exhibited chattering in its control signal, whereas the MSTSMC did not. This further demonstrates the

superiority of the MSTSMC, as it exhibits greater stability in its control signal. Similar to the previous test results, Table IV presents a comparison of performance metrics that provide computational and analytical proof that the MSTSMC produced smaller error values in terms of IAE, ISE, ITAE, and RMSE than the CSMC. The magnitude of the MSTSMC's control signal was also smaller than that of the CSMC. The smaller total variation of the MSTSMC indicates smaller chattering.

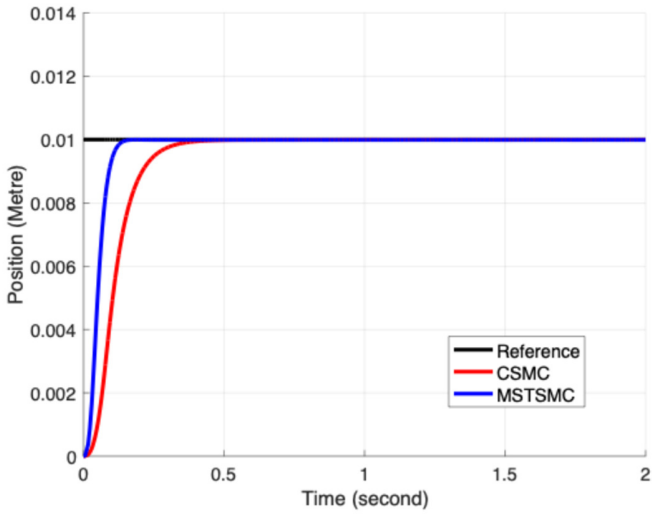

Fig. 7. Simulation results of CSMC and MSTSMC.

TABLE III. RESPONSE SYSTEM COMPARISON

Controller	t_r (s)	t_s (s)	O_s (%)	ss_e (m)
CSMC	0.1591	0.3140	0	0
MSTSMC	0.0697	0.1418	0	0

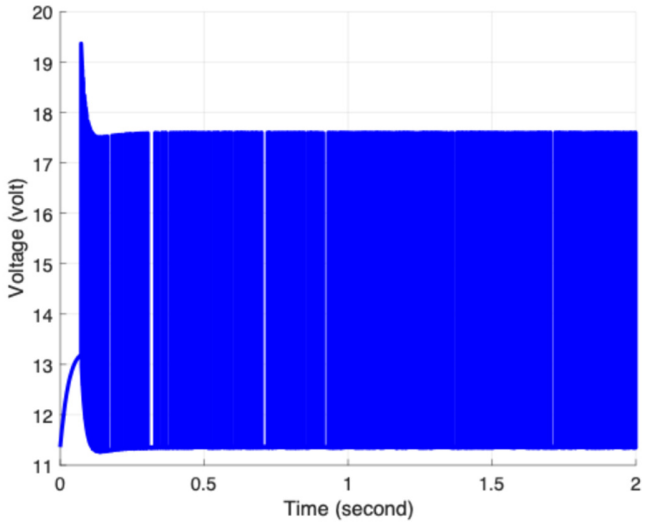

Fig. 8. Control signal of CSMC.

The improved performance of MSTSMC under resistance and inductance uncertainty is due to its switching action, which differs from that of CSMC. Variations in resistance and inductance directly affect the electrical dynamics, which modify the effective input gain and introduce matched uncertainty into the sliding-variable dynamics, $\dot{s}$. CSMC's discontinuous $sgn(s)$ switching enforces robustness, but it also amplifies high-frequency activity, resulting in chattering and increased sensitivity to unmodeled dynamics. In contrast, MSTSMC uses a continuous, higher-order switching mechanism (super-twisting action) that maintains strong disturbance rejection while producing a smoother control signal. This continuous correction reduces excitation of high-frequency modes and mitigates chattering. Thus, it yields more consistent transient and steady-state performance when R and L vary. The tabulated step-response metrics and control-signal plots quantitatively support this explanation, showing faster settling and reduced control variation for MSTSMC across uncertainty cases.

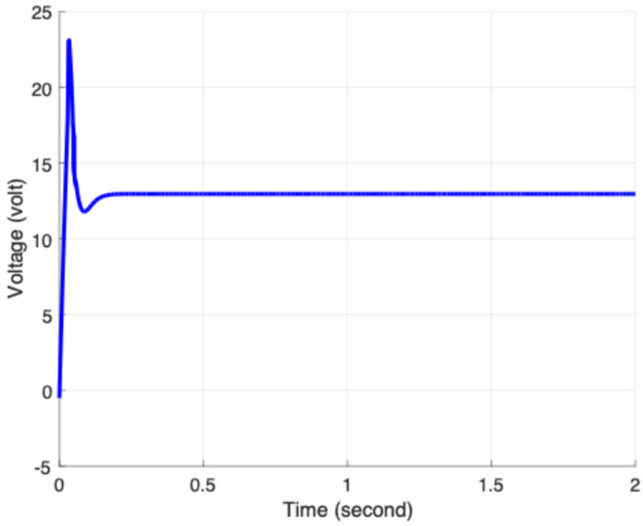

Fig. 9. Control signal of MSTSMC.

TABLE IV. PERFORMANCE METRICS COMPARISON

Controller	*IAE*	*ISE*	*ITAE*	*RMSE*	u_{RMS}	E_u	*TV*
CSMC	6.235e-06	9.662e-04	6.903e-05	0.0344	11.6814	436.4	26.96
MSTSMC	3.558e-06	5.02e-04	1.698e-05	0.0235	12.9425	420.1	21.34

IV. CONCLUSIONS

This paper presents a Modified Super-Twisting Sliding Mode Control (MSTSMC) strategy for the position regulation of a nonlinear Magnetic Levitation System (MLS) in the presence of coil resistance and inductance uncertainties. The simulation results demonstrate that the MSTSMC strategy achieves more accurate tracking and improved transient behavior compared to the Conventional Sliding Mode Control (CSMC) strategy. Additionally, the MSTSMC strategy produces a smoother control signal with significantly reduced chattering. The effectiveness of MSTSMC was further verified under variations in resistance and uncertainty parameters, where it maintained stable tracking and bounded error. Despite these promising results, the current study has several limitations. First, all findings are based on MATLAB/Simulink

simulations. Therefore, unmodeled dynamics, such as actuator saturation, sensor noise, quantization, delays, and thermal-electromagnetic coupling, may affect performance in practice. Second, the robustness assessment focused on uncertainty in electrical parameters. Additional disturbances, such as external vibrations and payload changes, and broader model mismatch, were not thoroughly examined. Future work should address these limitations by implementing the proposed controller in real time on an embedded platform and experimentally validating it on a laboratory MLS setup. Additional research may include systematic comparisons with other advanced nonlinear controllers, such as adaptive control, observer-based SMC, backstepping, feedback linearization, and higher-order sliding mode. The uncertainty study will also be extended to include combined disturbances, measurement noise, and actuator constraints.

DECLARATION OF COMPETING INTERESTS

The authors declare that they have no conflicts of interest.

ACKNOWLEDGMENT

The authors would like to thank the Indonesian Education Scholarships (BPI), the Center for Higher Education Funding and Assessment, Ministry of Higher Education, Science and Technology of the Republic of Indonesia, and the Indonesia Endowment Fund for Education (LPDP).

DATA AVAILABILITY

The data used to support the findings of this study are available at reasonable request from the corresponding author.

REFERENCES

[1] R. S. Gopi, S. Srinivasan, K. Panneerselvam, Y. Teekaraman, R. Kuppusamy, and S. Urooj, "Enhanced model reference adaptive control scheme for tracking control of magnetic levitation system," *Energies*, vol. 14, no. 5, 2021, Art. no. 1455, https://doi.org/10.3390/en14051455.

[2] A. Bizuneh, H. Mitiku, A. O. Salau, and K. Chandran, "Performance analysis of an optimized PID-P controller for the position control of a magnetic levitation system using recent optimization algorithms," *Measurement: Sensors*, vol. 33, 2024, Art. no. 101228, https://doi.org/10.1016/j.measen.2024.101228.

[3] J. Wang, L. Zhao, and L. Yu, "Adaptive terminal sliding mode control for magnetic levitation systems with enhanced disturbance compensation," *IEEE Transactions on Industrial Electronics*, vol. 68, no. 1, pp. 756–766, 2021, https://doi.org/10.1109/TIE.2020.2975487.

[4] A. T. Vo, T. N. Truong, and H. J. Kang, "A novel fixed-time control algorithm for trajectory tracking control of uncertain magnetic levitation systems," *IEEE Access*, vol. 9, pp. 47698–47712, 2021, https://doi.org/10.1109/ACCESS.2021.3068140.

[5] T. Gao, J. Yang, L. Jia, Y. Deng, W. Zhang, and Z. Zhang, "Design of new energy-efficient permanent magnetic maglev vehicle suspension system," *IEEE Access*, vol. 7, pp. 135917–135932, 2019, https://doi.org/10.1109/ACCESS.2019.2939879.

[6] Z. Huang *et al*., "Magnetic bearing: Structure, model, and control strategy," *The International Journal of Advanced Manufacturing Technology*, vol. 131, no. 5, pp. 3287–3333, 2024, https://doi.org/10.1007/s00170-023-12389-8.

[7] Y. Chen, Y. Zhang, and B. Cai, "Suspension strategy of maglev vertical axis wind turbine based on sliding mode adaptive neural network predictive control," *IEEE Access*, vol. 10, pp. 91712–91721, 2022, https://doi.org/10.1109/ACCESS.2022.3202924.

[8] M. Zhai, Z. Long, and X. Li, "A new strategy for improving the tracking performance of magnetic levitation system in maglev train," *Symmetry*, vol. 11, no. 8, 2019, Art. no. 1053, https://doi.org/10.3390/sym11081053.

[9] A. A. Ashkarran and M. Mahmoudi, "Magnetic levitation systems for disease diagnostics," *Trends in Biotechnology*, vol. 39, no. 3, pp. 311–321, 2021, https://doi.org/10.1016/j.tibtech.2020.07.010.

[10] B. Karakuzu *et al*., "Magnetic levitation-based miniaturized technologies for advanced diagnostics," *Emergent Materials*, vol. 7, no. 6, pp. 2323–2348, 2024, https://doi.org/10.1007/s42247-024-00762-6.

[11] S. R. Dabbagh, M. M. Alseed, M. Saadat, M. Sitti, and S. Tasoglu, "Biomedical applications of magnetic levitation," *Advanced NanoBiomed Research*, vol. 2, no. 3, 2022, Art. no. 2100103, https://doi.org/10.1002/anbr.202100103.

[12] M. N. Noaman, A. B. Ayoub, and S. S. Mahmood, "Nonlinear model predictive control of a magnetic levitation system using artificial protozoa optimizer," *International Journal of Robotics and Control Systems*, vol. 4, no. 4, pp. 1947–1966, 2024, https://doi.org/10.31763/ijrcs.v4i4.1668.

[13] K. Hu, J. Niu, Q. Jiang, J. Yang, and W. Zhang, "Magnetic levitation system control based on a novel tracking differentiator," *ISA Transactions*, vol. 151, pp. 350–362, 2024, https://doi.org/10.1016/j.isatra.2024.05.037.

[14] S. Chamraz, M. Huba, and K. Zakova, "Stabilization of the magnetic levitation system," *Applied Sciences*, vol. 11, no. 21, 2021, Art. no. 10369, https://doi.org/10.3390/app112110369.

[15] A. Demiroren, S. Ekinci, B. Hekimoγlu, and D. Izci, "Opposition-based artificial electric field algorithm and its application to FOPID controller design for unstable magnetic ball suspension system," *Engineering Science and Technology, an International Journal*, vol. 24, no. 2, pp. 469–479, 2021, https://doi.org/10.1016/j.jestch.2020.08.001.

[16] F. Li, Y. Sun, J. Xu, Z. He, and G. Lin, "Control methods for levitation system of EMS-type maglev vehicles: An overview," *Energies*, vol. 16, no. 7, 2023, Art. no. 2995, https://doi.org/10.3390/en16072995.

[17] Y. Zheng and H.-J. Ahn, "Improvement of the transient levitation response of a magnetic levitation system using hybrid fuzzy and artificial neural network control," *International Journal of Precision Engineering and Manufacturing*, vol. 26, no. 5, pp. 1159–1165, 2025, https://doi.org/10.1007/s12541-024-01173-7.

[18] O. Y. Ismael, Y. H. S. Alnema, A. H. Hameed, and A. J. Humaidi, "Robust control of a magnetic levitation system via LESO-based feedback linearization tuned by modified flood algorithm," *International Journal of Dynamics and Control*, vol. 14, no. 1, 2026, Art. no. 14, https://doi.org/10.1007/s40435-025-01904-2.

[19] O. D. Montoya Giraldo, W. Gil-González, and A. Jaramillo-Matta, "A generalized backstepping controller design for a second-order magnetic levitation system," *Statistics, Optimization and Information Computing*, vol. 13, no. 1, pp. 286–296, 2025, https://doi.org/10.19139/soic-2310-5070-2205.

[20] A. Zemouche, F. Zhang, F. Mazenc, and R. Rajamani, "High-gain nonlinear observer with lower tuning parameter," *IEEE Transactions on Automatic Control*, vol. 64, no. 8, pp. 3194–3209, 2019, https://doi.org/10.1109/TAC.2018.2882417.

[21] W. Yang, F. Meng, M. Sun, and K. Liu, "Passivity-based control design for magnetic levitation system," *Applied Sciences*, vol. 10, no. 7, 2020, Art. no. 2392, https://doi.org/10.3390/app10072392.

[22] A. K. Ahmed, H. Al-Khazraji, O. F. Lutfy, and A. S. Al-Araji, "Comparative analysis of control strategies for tracking periodic sinusoidal references in magnetic levitation systems," *International Journal of Robotics and Control Systems*, vol. 5, no. 4, pp. 2325–2343, 2025, https://doi.org/10.31763/ijrcs.v5i4.2116.

[23] O. Y. Ismael, M. Qasim, and M. N. Noaman, "Equilibrium optimizer-based robust sliding mode control of magnetic levitation system," *Journal Européen des Systèmes Automatisés*, vol. 54, no. 1, pp. 131–138, 2021, https://doi.org/10.18280/jesa.540115.

[24] T. T. Pham and N. T. Pham, "A hybrid PI–SOSM control strategy with disturbance observer for enhanced dynamic response of IM drives," *Buletin Ilmiah Sarjana Teknik Elektro*, vol. 7, no. 4, pp. 702–714, 2025, https://doi.org/10.12928/biste.v7i4.14458.

[25] Y. Zahraoui, M. Akherraz, and A. Ma'arif, "A comparative study of nonlinear control schemes for induction motor operation improvement," *International Journal of Robotics and Control Systems*, vol. 2, no. 1, pp. 1–17, 2022, https://doi.org/10.31763/ijrcs.v2i1.521.

[26] A. Hasni *et al*., "Optimized speed regulation of BLDC motors: A comparative performance study of artificial neural networks and super-twisting sliding mode controllers," *International Journal of Robotics and Control Systems*, vol. 5, no. 4, pp. 2360–2378, 2025, https://doi.org/10.31763/ijrcs.v5i4.2046.

[27] T. L. Huu, H. L. Anh, and D. T. Tran, "Applying Sliding Mode Control to a Quadrotor," *Engineering, Technology & Applied Science Research*, vol. 14, no. 5, pp. 16389–16394, Oct. 2024, https://doi.org/10.48084/etasr.8026.

[28] A. Daadi *et al*., "Sliding mode controller based on the sliding mode observer for a QBall 2+ quadcopter with experimental validation," *International Journal of Robotics and Control Systems*, vol. 2, no. 2, pp. 332–356, 2022, https://doi.org/10.31763/ijrcs.v2i2.693.

[29] M. S. Mahmoud, R. A. A. Saleh, and A. Ma'arif, "Stabilizing of inverted pendulum system using robust sliding mode control," *International Journal of Robotics and Control Systems*, vol. 2, no. 2, pp. 230–239, 2022, https://doi.org/10.31763/ijrcs.v2i2.594.

[30] I. Hassani, I. Ergui, and C. Rekik, "Turning point and free segments strategies for navigation of wheeled mobile robot," *International Journal of Robotics and Control Systems*, vol. 2, no. 1, pp. 172–186, 2022, https://doi.org/10.31763/ijrcs.v2i1.586.

[31] K. Cherif, A. Sahbani, and K. B. Saad, "Performance Evaluation of PI and Sliding Mode Control for PMSM in Applications for Electric Vehicles," *Engineering, Technology & Applied Science Research*, vol. 14, no. 4, pp. 15464–15470, Aug. 2024, https://doi.org/10.48084/etasr.7172.

[32] M. G. Ghogare, A. R. Laware, S. L. Patil, and C. Y. Patil, "Design and analysis of decentralized dynamic sliding mode controller for TITO process," *International Journal of Robotics and Control Systems*, vol. 2, no. 2, pp. 277–296, 2022, https://doi.org/10.31763/ijrcs.v2i2.648.

[33] Q.T. Tran, "Control of a Grid-connected Inverter using Sliding Mode Control," *Engineering, Technology & Applied Science Research*, vol. 14, no. 3, pp. 14558–14565, June 2024, https://doi.org/10.48084/etasr.7335.

[34] O. J. Tola, E. A. Umoh, E. A. Yahaya, and O. E. Olusegun, "Permanent magnet synchronous generator connected to a grid via a high speed sliding mode control," *International Journal of Robotics and Control Systems*, vol. 2, no. 2, pp. 379–395, 2022, https://doi.org/10.31763/ijrcs.v2i2.701.

[35] A. Al-Ataby and H. Attia, "A Sliding Mode Controller Design for Buck Converters in Robotic Power Systems," *Engineering, Technology & Applied Science Research*, vol. 15, no. 5, pp. 27885–27892, Oct. 2025, https://doi.org/10.48084/etasr.13015.

[36] L. Yu, J. Huang, W. Luo, S. Chang, H. Sun, and H. Tian, "Sliding-mode control for PMLSM position control—A review," *Actuators*, vol. 12, no. 1, 2023, Art. no. 31, https://doi.org/10.3390/act12010031.

[37] H. Komurcugil, S. Biricik, S. Bayhan, and Z. Zhang, "Sliding mode control: Overview of its applications in power converters," *IEEE Industrial Electronics Magazine*, vol. 15, no. 1, pp. 40–49, 2021, https://doi.org/10.1109/MIE.2020.2986165.

[38] V. Utkin, A. Poznyak, Y. Orlov, and A. Polyakov, "Conventional and high order sliding mode control," *Journal of the Franklin Institute*, vol. 357, no. 15, pp. 10244–10261, 2020, https://doi.org/10.1016/j.jfranklin.2020.06.018.

[39] S. Ullah, A. Mehmood, Q. Khan, S. Rehman, and J. Iqbal, "Robust integral sliding mode control design for stability enhancement of under-actuated quadcopter," *International Journal of Control, Automation and Systems*, vol. 18, no. 7, pp. 1671–1678, 2020, https://doi.org/10.1007/s12555-019-0302-3.

[40] M. Saghafi Zanjani and S. Mobayen, "Anti-sway control of offshore crane on surface vessel using global sliding mode control," *International Journal of Control*, vol. 95, no. 8, pp. 2267–2278, 2022, https://doi.org/10.1080/00207179.2021.1906447.

[41] H. M. S. Yaseen, S. A. Siffat, I. Ahmad, and A. S. Malik, "Nonlinear adaptive control of magnetic levitation system using terminal sliding mode and integral backstepping sliding mode controllers," *ISA Transactions*, vol. 126, pp. 121–133, 2022, https://doi.org/10.1016/j.isatra.2021.07.026.

[42] P. Roy and B. K. Roy, "Sliding mode control versus fractional-order sliding mode control: Applied to a magnetic levitation system," *Journal of Control, Automation and Electrical Systems*, vol. 31, no. 3, pp. 597–606, 2020, https://doi.org/10.1007/s40313-020-00587-8.

[43] F. M. Zaihidee, S. Mekhilef, and M. Mubin, "Robust speed control of PMSM using sliding mode control: A review," *Energies*, vol. 12, no. 9, 2019, Art. no. 1669, https://doi.org/10.3390/en12091669.

[44] H. M. M. Adil, S. Ahmed, and I. Ahmad, "Control of MagLev system using supertwisting and integral backstepping sliding mode algorithm," *IEEE Access*, vol. 8, pp. 51352–51362, 2020, https://doi.org/10.1109/ACCESS.2020.2980687.

[45] Y. Zahraoui, M. Moutchou, S. Tayane, C. Fahassa, and S. Elbadaoui, "Induction motor performance improvement using super twisting SMC and twelve sector DTC," *International Journal of Robotics and Control Systems*, vol. 4, no. 1, pp. 50–68, 2024, https://doi.org/10.31763/ijrcs.v4i1.1090.

[46] L. Wu *et al*., "Sliding mode control in power converters and drives: A review," *IEEE/CAA Journal of Automatica Sinica*, vol. 9, no. 3, pp. 392–406, 2022, https://doi.org/10.1109/JAS.2021.1004380.